fNIRS-based online deception decoding

2012 J. Neural Eng. 9 026012

(http://iopscience.iop.org/1741-2552/9/2/026012)

J. Neural Eng. **9** (2012) 026012 (8pp) doi:10.1088/1741-2560/9/2/026012

fNIRS-based online deception decoding

Xiao-Su Hu[1], **Keum-Shik Hong**[1,2,4] **and Shuzhi Sam Ge**[1,3]

[1] Department of Cogno-Mechatronics Engineering, Pusan National University, 30 Jangjeon-dong, Gumjeong-gu, Busan 609-735, Korea
[2] School of Mechanical Engineering, Pusan National University, 30 Jangjeon-dong, Gumjeong-gu, Busan 609-735, Korea
[3] Department of Electrical & Computer Engineering, National University of Singapore, Singapore

E-mail: kshong@pusan.ac.kr

Received 22 November 2011
Accepted for publication 18 January 2012
Published 16 February 2012
Online at stacks.iop.org/JNE/9/026012

Abstract
Deception involves complex neural processes in the brain. Different techniques have been used to study and understand brain mechanisms during deception. Moreover, efforts have been made to develop schemes that can detect and differentiate deception and truth-telling. In this paper, a functional near-infrared spectroscopy (fNIRS)-based online brain deception decoding framework is developed. Deploying dual-wavelength fNIRS, we interrogate 16 locations in the forehead when eight able-bodied adults perform deception and truth-telling scenarios separately. By combining preprocessed oxy-hemoglobin and deoxy-hemoglobin signals, we develop subject-specific classifiers using the support vector machine. Deception and truth-telling states are classified correctly in seven out of eight subjects. A control experiment is also conducted to verify the deception-related hemodynamic response. The average classification accuracy is over 83.44% from these seven subjects. The obtained result suggests that the applicability of fNIRS as a brain imaging technique for online deception detection is very promising.

(Some figures may appear in colour only in the online journal)

1. Introduction

Deception is a cognitively demanding process requiring intentional suppression of the truth, interactive communication and strategic modifications of behaviors to convince the receiver. Various techniques have been developed to detect deceptions. One typical method is the polygraph (Brett *et al* 1986, Honts *et al* 1994, Mohamed *et al* 2006). However, this method is an indirect method that can detect arousal from the peripheral nervous system but not the brain response. Direct methods were also developed, which include electroencephalography (EEG) and functional magnetic resonance imaging (fMRI). EEG has been utilized to test special knowledge, for instance, the guilty knowledge test (GKT) (Farwell and Donchin 1991). The GKT is a test of prior knowledge of crime details that would be known only to the suspect involved in the crime (Elaad and Benshakhar 1991, 1997, Furedy and Benshakhar 1991, Elaad 1997). Although EEG provides high temporal resolution for detecting neuronal signals, it is difficult to localize the source of the potential associated with the deception process. Compared to EEG, the blood oxygen level-dependent fMRI offers much greater spatial resolution (Huettel *et al* 2008). It can localize the changes in regional cerebral blood flow (rCBF) that are associated with increased neuronal activation.

Taking advantage of fMRI's high spatial resolution, the deception-related brain regions were investigated by multiple research groups (Spence *et al* 2001, 2004, Langleben *et al* 2002, 2005, Lee *et al* 2002, Ganis *et al* 2003, Kozel *et al* 2004a, 2004b, 2005, 2009a, 2009b, Nunez *et al* 2005, Phan *et al* 2005, Mohamed *et al* 2006). The prefrontal cortex was observed in a number of studies reporting that a greater activation exists during deception as compared to the control condition of telling the truth. Answering truthfully was believed to be a state requiring less cognitive control than lying according to these studies. Specifically, recent studies using fMRI have achieved reliable results in differentiating the deceptive response from that of truth-telling at an individual level under laboratory

[4] Author to whom any correspondence should be addressed.

conditions (Kozel *et al* 2005, 2009a, 2009b, Langleben *et al* 2005).

However, the non-portability and the high cost of fMRI scanners limit the use of fMRI technologies in many cases. Moreover, fMRI is known to be extremely sensitive to motion artifacts. Therefore, some researchers started to look for an alternative brain imaging technique, functional near-infrared spectroscopy (fNIRS). fNIRS measures the hemodynamic changes that effectively reflect the brain activities occurring while people perform a wide range of mental tasks (Koizumi *et al* 2003, Obrig and Villringer 2003, Boas *et al* 2004, Wolf *et al* 2007, Perrey 2008). It can provide both topographic (Koizumi *et al* 2003, Toronov *et al* 2007, Wolf *et al* 2007, Hu *et al* 2011) and tomographic (Barbour *et al* 2001, Boas *et al* 2004) brain images. Specifically, fNIRS monitors the rCBF variation by measuring, through the skull, the absorption changes of near-infrared light at wavelengths between 650 and 950 nm (Obrig and Villringer 2003). These changes are caused by the concentration variations of oxy-hemoglobin (HbO) and deoxy-hemoglobin (HbR), two primary absorbing chromophores in brain capillary blood.

fNIRS, compared with other prevalent brain imaging techniques such as EEG and fMRI, offers a good trade-off between spatial and temporal resolutions. The usability and drawbacks of fNIRS, in comparison with other neuroimaging methods, were discussed and analyzed by Perrey (2008). Another comprehensive review (Irani *et al* 2007) comparing respective features of fNIRS and fMRI concluded that fNIRS has great potentials for neurological and psychiatric applications due to its simplicity, portability and insensitivity to motion artifacts compared with fMRI. Meanwhile, the EEG technique is limited, due to its poor spatial resolution and low signal-to-noise ratio in many applications (Turnip *et al* 2011). From these aspects, fNIRS can provide comparatively better quality (Gratton and Fabiani 2001a). An increasing number of researchers are focusing on using fNIRS to decode mental states and to develop a brain–computer interface (BCI): a detailed review of BCI was provided in Sitaram *et al* (2009).

fNIRS is capable of detecting brain signals in the cortical layer, whereas several fMRI studies indicated that some neural pathways in the prefrontal cortex become critical during deception. A recent study has explored the utilization of fNIRS for deception detection, and supported that fNIRS has great potential in this area: Tian *et al* (2009) reported an interesting result of deception detection with a mock theft scenario. They analyzed both HbO and HbR signals during a deception state, and compared them with those during a truth-telling state (control condition). They also conducted an offline classification study for identifying different objects that the subject took. Their study indicated that there were significant responses at the prefrontal cortex during the deception period demonstrating the development of an fNIRS-based framework for deception decoding.

In this paper, an online fNIRS-based framework for decoding intentional deceptions is developed. For deception decoding, both preprocessed HbO and HbR signals with their recent histories are further analyzed. It is demonstrated that a classifier trained by the support vector machine (SVM) algorithm can identify a deception state approximately 3.12 s after the beginning of the state. A mock theft scenario similar to that designed in the fMRI study (Kozel *et al* 2005) for deception detection is used in this study. The contributions of this paper are: (i) this paper presents the first work on an online deception classification algorithm based upon fNIRS. (ii) With the developed fNIRS technique, a collaborative performance between left and right prefrontal cortices during deception period could be demonstrated. (iii) The signal history was included into the feature space to reduce the classification time.

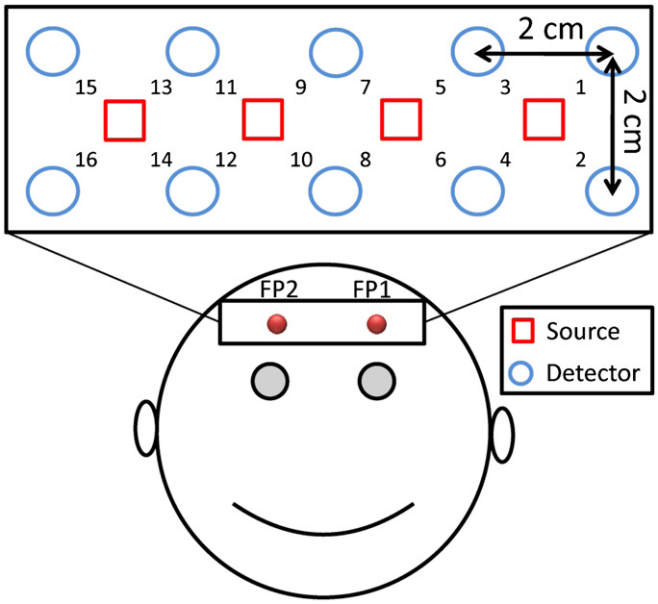

Figure 1. Source/detector locations and channel distribution: two reference points (FP1 and FP2) confirm the International 10-20 System.

2. Materials and methods

2.1. Experimental paradigm

Eight right-handed healthy volunteers (all males, aged 24 to 34 years) participated in the experiment. None of the participants had a history of any neurological disorder. All of the participants provided written informed consent. The experiment was conducted in accordance with the latest Declaration of Helsinki. The data were acquired with a continuous-wave NIRS imaging system (DYNOT: dynamic near-infrared optical tomography) developed by NIRx Medical Technologies, Brooklyn, NY, at a sampling rate of 1.81 Hz. The system emits laser light of two wavelengths (760 and 830 nm) from each source. Figure 1 shows the channel distribution and measurement location.

The paradigm uses a mock theft scenario similar to that given by Kozel *et al* (2005). The participant is instructed to 'steal' a watch or a ring from a drawer (in this study, four persons took a watch and the other four took a ring). The selected item is kept unknown to the investigator, and placed in an envelope on a table. Then the participant put the fNIRS probe on his forehead with the assistance of the investigator.

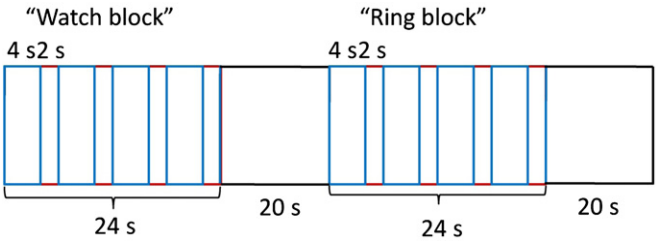

Figure 2. The used experimental paradigm: one session consists of two question blocks ('watch' and 'ring' blocks). In each block, four questions are presented followed by a rest period of 20 s. Each question takes 4 s, and its answering time is 2 s. The entire experiment is composed of five sessions (two training sessions and three testing sessions).

Before the formal deception test, the participant performs a practice task, which consists of an instruction slide and questions with a clear 'Yes' or 'No' answer. The questions are presented on a computer screen, and the participants are asked to respond to the question by pressing 'Key 1' or 'Key 2' on the keyboard ('Yes' or 'No' answer) using their left hand. This practice process enables the subjects to get familiar with the question presentation as well as the keyboard response with fingers. During the experiment, the participant is required to answer two categories of questions (see the appendix) presented on the computer screen: 'ring' questions regarding whether he took the ring; 'watch' questions regarding whether he took the watch. The answers to questions regarding ring and watch would be either lies or truths depending on the object the participant selected.

Each question slide is presented for 4 s on the screen, followed by a prompt slide asking the subject to answer 'Yes or No' via key stroke. The prompt slide stays on the screen for 2 s. Each category contains 20 questions, and thus 40 questions are presented. In this work, a blocked design was adopted during the question presentation. Twenty questions in the same category were split into five blocks, with an interval of 20 s between each block. The timing sequence of one session in the experimental paradigm is shown in figure 2. A session is defined as the combination of a block involving a 'watch' question block followed by a rest period for 20 s, followed by a 'ring' question block and followed by another rest period. The whole experiment includes five sessions. For comparison purpose, another experiment was conducted using the same experimental paradigm. The same questions were presented to the second group of subjects (eight subjects) without taking any object from the drawer. The relevant hemodynamic response was recorded and further analyzed.

2.2. Signal analysis

2.2.1. Measurement model for fNIRS. In fNIRS measurement, the optical density variation (ΔOD) can be modeled as a linear combination of hemoglobin concentration changes (Δc_{HbO} and Δc_{HbR}) multiplied by proper coefficients. Their relationship is described by the modified Beer–Lambert law (MBLL), a law relating the reduction in luminous intensity of light passing through a material to the length of the light's path through the material, as

$$\Delta \mathrm{OD}^i(\lambda) = (a_{\mathrm{HbO}}(\lambda)\Delta c_{\mathrm{HbO}} + a_{\mathrm{HbR}}(\lambda)\Delta c_{\mathrm{HbR}})L^i \mathrm{DPF}(\lambda), \tag{1}$$

where λ is the wavelength of the laser source, the superscript i indicates the index of channels, a_{HbO} ($\mu\mathrm{M}^{-1}$ mm^{-1}) and a_{HbR} ($\mu\mathrm{M}^{-1}$ mm^{-1}) are the extinction coefficients of the HbO and HbR, L^i is the distance between the source and the detector of the ith channel and DPF is the differential path length factor. In this paper, the optical density data are first converted to the hemoglobin concentration change data via MBLL. The data series detected from all the channels are then preprocessed using a band-pass filter (elliptic filter) with 0.01 and 0.2 Hz cutoff frequencies.

2.2.2. Features. fNIRS is unique, among neuroimaging technologies, because it can provide both HbO and HbR concentration levels simultaneously at each location. In this study, we include both HbO and HbR signals into the feature space for detecting deception (it is found that the HbO level increases and the HbR level decreases during deception, while both levels are normal during truth-telling or rest). Moreover, short histories (previous data) of the HbO and HbR signals are also considered together with the event-related data: 1, 3 and 5 s history of the data prior to the current time. We then compare the classification performances to investigate a proper size of data history for deception decoding.

In this study, we adopt the contrast-to-noise ratio (CNR) to quantify the signal-to-noise ratio (Cui *et al* 2010), and select efficient channels for further classification based on the training data set. We use the first two sessions for training the model, and the rest three sessions are used as a testing set. Basically, the CNR calculates the amplitude difference between the averaged signals during active periods, divided by the pooled standard deviation. A larger CNR indicates that the ratio of deception-related signal to noise is larger.

$$\mathrm{CNR} = \frac{\left|\sum \mathrm{mean}_{\mathrm{HBX}}(\mathrm{active})\right| - \left|\sum \mathrm{mean}_{\mathrm{HBX}}(\mathrm{rest/inactive})\right|}{\sqrt{\sum v\mathrm{ar}_{\mathrm{HBX}}(\mathrm{active}) + \sum \mathrm{var}_{\mathrm{HBX}}(\mathrm{rest/inactive})}}, \tag{2}$$

where 'active' refers to the period of deception, and 'rest/inactive' means the rest period and truth-telling period, we then compare the classification performance using only selected channels with the one using all the channels to investigate an optimal channel combination.

2.2.3. Support vector machine. The classification task is based on the training data and the testing data involving several sessions of data. The data at each time point in the training set contain one target value, that is, the class type and its attributes. The objective of the SVM is to produce a model according to the training set, and this model is used to predict the target values in the testing set when only the attributes are given. At each time instance k, the classification problem is to determine a scalar y_k (target value) from a measurement vector $\boldsymbol{X}_k$ (attributes). In the classification of the fNIRS data

from multiple channels at both hemispheres, $\boldsymbol{X}_k$ represents the concentration values of HbO and HbR measured from different channels with their recent histories. In this study, y_k is 1 when the subject is doing the deception task and 0 when he is telling the truth or having a rest. This work is restricted to the binary classification.

In the formulation of the SVM, with a nonlinear kernel, the input vector $\boldsymbol{X}_k$ is mapped to a high dimensional feature space, $\boldsymbol{Z}_k$, through a nonlinear transformation function $g(\cdot)$, so that $\boldsymbol{Z}_k = g(\boldsymbol{X}_k)$. The SVM algorithm attempts to find a decision boundary or a separating hyper-plane in the feature space, given by the decision function $D(\cdot)$:

$$D(Z_k) = \langle W, Z_k \rangle + \omega, \tag{3}$$

where ω represents the intercept, and the parameter $\boldsymbol{W}$ can be obtained by solving the equation

$$y_k(\langle W, Z_k \rangle + \omega) > 1 - \xi. \tag{4}$$

Under the constraint, the solution becomes optimal when $\frac{1}{2}W^T W + C \cdot f(\xi)$ is minimized, where ξ represents the training error, and the parameter C is the regularization constant, chosen by the user. A large value of C corresponds to higher penalty for classification errors.

In this study, we implemented the SVM classifier using the LibSVM package (Chang and Lin 2011). The LibSVM package is a C++ implementation, providing various features for SVM classification. The implementation was carried out in the following steps.

(a) fNIRS data were transformed into the format of LibSVM software. The training sets and testing sets were created as vectors of real numbers of HbO and HbR concentration changes at a specific time point with their recent history from 16 channels, while the subjects were doing deception, rest, or truth-telling. In order to compare the classification performance, we considered three different data history lengths (1, 3, 5 s); thus the dimensions of the feature vectors were 32 (16 channels $\times$ 2 levels), 204 (3 s $\times$ 1.8 Hz $\times$ 16 channels $\times$ 2 levels + 32) and 320 (5 s $\times$ 1.8 Hz $\times$ 16 channels $\times$ 2 levels + 32).

(b) Each attribute was scaled to a value in the range of $[-1, 1]$. The main reason for scaling is to avoid attributes having large numerical values.

(c) The kernel for the SVM algorithm was selected: radial basis function (RBF) kernel and linear kernel were both considered, and their performances were compared.

(d) The best penalty parameter C and kernel parameter using the LibSVM software for each subject were found. We performed a five-fold cross-validation to determine the classification accuracy. The cross-validation procedure is also known to prevent the over-fitting problem.

(e) The above parameters were used to train a SVM model for a specific subject.

(f) After training the model, the SVM model was used to predict the class label based on the attributes in the testing set.

2.2.4. The delay calculation and the classification accuracy. In this study, we report two kinds of delay, the onset delay and the offset delay. The onset delay is defined as the time between the onset of the subject deception and the first instance classified as 'active', while the offset delay is defined as the time from the offset of the subject deception to the status classified as 'inactive'. We also analyze both the inter-subject accuracy and intra-subject accuracy. The inter-subject accuracy is defined as the ratio of the correct classifications to the total classifications on the objects that a subject takes, while the intra-subject accuracy is defined as the ratio of the correct classifications to the total classifications on the state (deception versus truth-telling or rest) at each time point for each subject.

3. Results

Figure 3 shows the normalized, block-averaged hemodynamic responses (HbO and HbR data) of seven subjects in the main experiment and eight subjects in the control experiment, respectively, during deception, truth-telling and rest periods. The classification accuracies of all the subjects in the main experiment are shown in table 1. Subject 1 achieved the highest classification accuracy with both RBF kernel and linear kernel. The average intra-subject classification accuracy over all the subjects is 83.44% with the RBF kernel, and 81.14% with the linear kernel, as shown in table 1, while the inter-subject classification accuracy is 87.5% (seven out of eight subjects). Furthermore, we found that the classification accuracy is higher when using the data from all the channels, and the inclusion of 3 s data history is optimal. The comparison results are shown in figure 4.

4. Discussion

4.1. Differentiating between deception and truth-telling

In this paper, we attempted to classify a deception state from a truth-telling state online using the signals measured from the prefrontal cortex. The encouraging classification accuracies using the preprocessed HbO and HbR signals and the pre-trained SVM model warrant further investigation on a fNIRS-based online deception detection framework. We used the amplitudes of HbO and HbR with their recent temporal amplitude history as features for classification. The whole study was conducted under laboratory conditions. Block design is also used in this study. The purpose of using block design is to increase the signal-to-noise ratio of fNIRS.

A number of previous studies have reported that the prefrontal cortex is an important location where brain activities happen when the subject tells a lie. In this paper, we found that a significant deception-related brain activity exists at the left border of the left prefrontal cortex (channel 1) and the right anterior prefrontal cortex (channels 11, 13, and 14), as shown in figure 3. Clear hemodynamic responses regarding deception can be viewed in the upper panels compared with the lower panels in the data of the control experiment. This leads to the conclusion that collaboration between the left and right prefrontal cortices exists for a deception task.

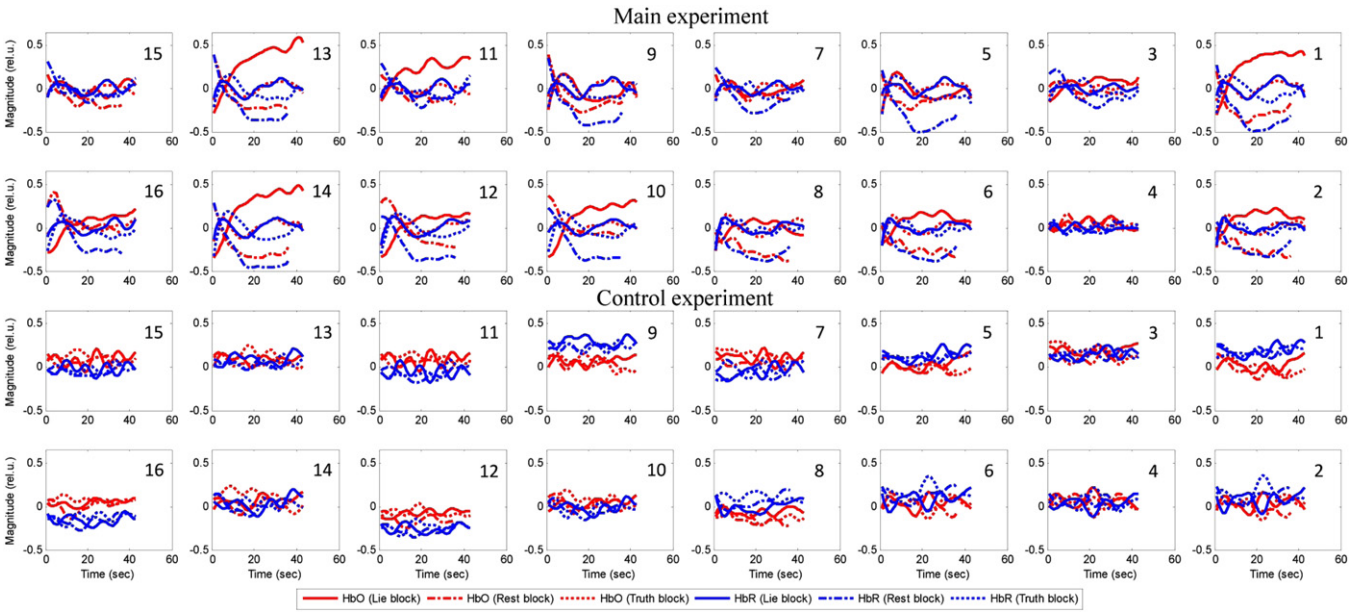

Figure 3. Comparison of six averaged hemodynamic responses (i.e. HbO-lie, HbO-rest, HbO-truth, HbR-lie, HbR-rest, and HbR-truth concentration changes) for 16 channels. The upper part shows the averages of 35 signals (five sessions in the main experiment, seven subjects) and the lower part depicts the averages of 40 signals (five sessions in the control experiment, eight subjects).

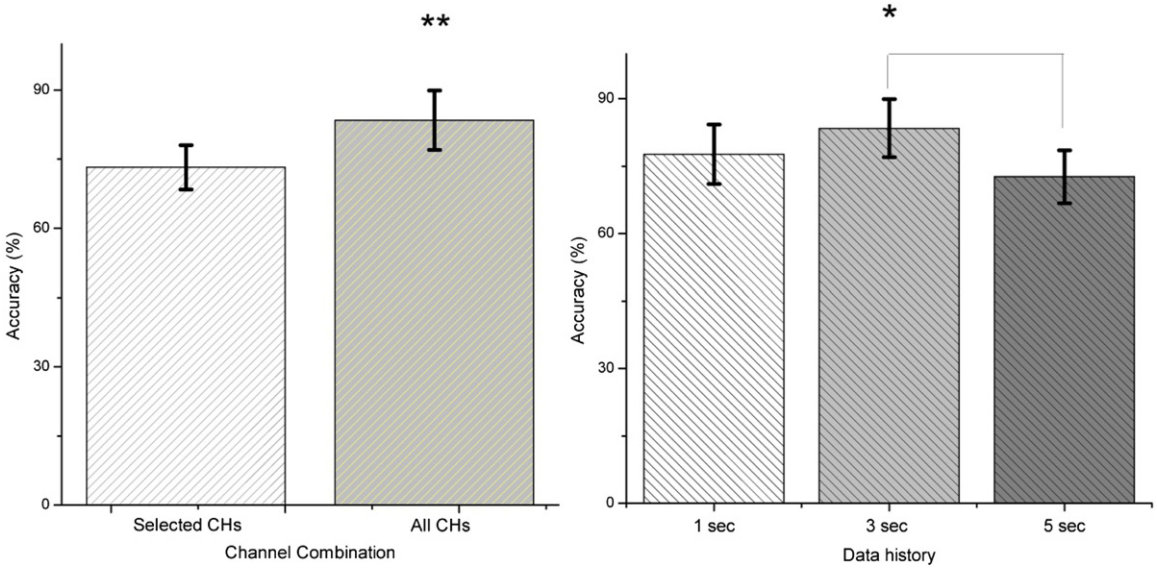

Figure 4. Comparison of classification accuracies: the two bar charts on the left-hand side show that the classification accuracy obtained by using all 16 channels is significantly higher than the one obtained by using only 6–10 selected channels from the CNR criteria. The three bar charts on the right-hand side indicate that the classification accuracy using 3 s data history is higher than those using 1 or 5 s data histories (*t*-test of **, $p < 0.005$; *t*-test of *, $p < 0.01$).

Table 1. The classification accuracy and delays for all the subjects (the asterisk indicates that the data are derived with the linear kernel).

Subject number	Object	Onset delay (S)	Offset delay (S)	Intra-subject classification accuracy with the RBF kernel (%)	Intra-subject classification accuracy with the linear kernel (%)
1	Watch	2.58*	1.10*	90.78	95.60
2	Watch	9.95	−7.18	75.42	73.17
3	Watch	1.12	1.66	86.30	62.38
4	Ring	3.25	2.38	75.31	62.89
5	Ring	2.76*	4.05*	82.07	87.79
6	Ring	1.05*	3.31*	84.26	93.37
7	Ring	1.12*	3.13*	82.16	92.59
Average		3.12	1.21	83.44	81.14
8	Watch	–	–	44.64	47.95

In this study, we train the subject-specific models for predicting their state at single time point. Our model can predict different brain states including active state (deception state) and inactive state (rest/truth-telling state), thus provide information for discriminating the different objects that a subject took. While 9 out 11 subjects were successfully classified in Tian *et al* (2009), 7 out of 8 subjects were successfully classified in our study. The inter-subject classification accuracy is at the same level compared with Tian *et al* (2009). The signals measured from the subject yielding an incorrect classification result showed no difference between the 'watch'-related question blocks and the 'ring' question blocks. The same subject reported loss of concentration while the experiment was running. Furthermore, our results achieved a similar inter-subject classification accuracy when compared with the conventional polygraph, but it was slightly lower than the level (90–93%) in a previous fMRI study (Kozel *et al* 2005). The reason might be that in the latter case, the total subjects' population was 61 (about eight times larger than ours). We therefore expect that the classification accuracy gets higher if the sample size gets larger.

We compared the performance of the RBF kernel with the one using the linear kernel. The average classification accuracies of two different kernels are similar according to the data in table 1. For four subjects, the performance using the linear kernel is better than the one using the RBF kernel while, for the other three, the performance using the RBF kernel is better than the one using the linear kernel. This result suggests that the feature dimension is not high enough to be linearly separable for some subjects, and thus the performance using the linear kernel is less stable than that using the RBF kernel.

4.2. Subjective memory suppression

We asked the subject to describe their mental image when telling a lie, after they finished their experiment. Interestingly, different subjects reported different mental images for conducting the deception task. Some subjects reported remembering the truth but choosing an opposite answer. A subject reported that he tried to avoid imaging the object (watch or ring) that he put in the envelope. Another subject reported imaging that the 'stolen' object still stays in the drawer. Because the underlying neurophysiological correlation of deception or truth-telling is beyond the scope of this study, such differences across subjects are acceptable and expected. As a result of inter-subject variability in hemodynamic response patterns, individualized model training has been recognized as necessary in the fNIRS decoding of cognitive states at the current stage.

4.3. The classification rate with different channel numbers and data history

We used the CNR to select the channels with a high response to the deception state for further classification. We compared the classification performance using the data from all the channels with the one using only selected channels. The results show that using all the channels is the best choice. This result can be interpreted as that the data measured from every channel include their own information that contributes to the signal classification. Meanwhile, the SVM is a classifier that can deal with a large data dimension. Therefore, the classification accuracy increases if the information reflected by the hemodynamic responses from all the channels are included in the feature space. The comparison results are shown in the left panel of figure 4.

We included the recent temporal data history into the feature space for classification. As discussed in Cui *et al* (2010), the temporal data history is very useful for increasing the intra-subject classification accuracy. We compared the results with different data history lengths, that is, 1, 3 and 5 s data length. The results show that the 3 s data history length is the optimal choice. The comparison among three histories is shown in the right panel, figure 4. It is remarked that the data history cannot be too short or too long for the online deception classification.

4.4. Onset and offset delay in deception identification

The response delay due to the hemodynamic response is a major limitation for fNIRS decoding cognitive states (for BCI). Many efforts have been put into how to shorten the response delays (Coyle *et al* 2007, Cui *et al* 2010). In this work, we are able to get the shortest onset delay of 1.12 s and the offset delay of 1.10 s, using the features of HbO and HbR with their recent history, 16 channels and a sampling rate at 1.81 Hz. These features make the classification time shorter, compared with other fNIRS decoding cognitive state studies (Coyle *et al* 2007, Sitaram *et al* 2007). In future work, we will test a different feature combination, increase the number of channels and increase the data sampling frequency to investigate whether the classification delays can be further shortened. Moreover, recent studies (Gratton and Fabiani 2001b, Hu *et al* 2011) suggest that such a time period might be shortened by employing fast optical responses.

4.5. Limitation of the proposed scheme

Many researchers used fMRI for brain-signal-based deception research by taking advantage of fMRI's high spatial resolution. However, fNIRS was used in this study to decode deception as it has higher temporal resolution compared with fMRI. The higher temporal resolution allows us to develop an online framework. The proposed framework considers the recent signal history as a classification feature. This feature makes the classification time shorter, compared with other fNIRS decoding cognitive state studies (Coyle *et al* 2007, Sitaram *et al* 2007).

However, there are several limitations in this study. Sitaram *et al* (2009) proposed two important questions for fNIRS decoding cognitive state studies in general: (i) is it possible to perform brain state classification automatically based on the subjects' brain activity? (ii) Is it possible to do this online, or in real-time as against after several minutes or days of offline processing? In this study, only a simulated online environment was used. The data were incorporated sequentially for classification. To modify the framework online

in reality, first, an online data acquiring interface needs to be added to the framework. Many previous works reported a successful online data acquiring interface (Abdelnour and Huppert 2009, Coyle *et al* 2007). Second, online data filtering methods need to be applied. Cui and co-workers (2010) applied exponential moving average to the fNIRS data, whereas our previous work (Hu *et al* 2010) applied Kalman filtering to the fNIRS data.

Another limitation of this framework is the subject-specific SVM models. In order to apply this framework in reality, a short calibration procedure for the model needs to be derived. In this study, a long calibration procedure of the SVM model was of 176 s. Under the background to deception detection in criminal or other cases, a model with a short calibration procedure is required. Future research will focus on how to shorten the calibration procedure.

Finally, the proposed framework needs to be further validated. Our purpose is to develop a generalized framework for online deception detection for criminal or other cases. In this paper, only male subjects from age 24 to 34 were tested. In future work, female subjects, old people and children need to be investigated to confirm the generalized feasibility of the proposed framework.

5. Conclusion

A fNIRS-based online deception decoding framework was proposed in this paper. The HbO and HbR signals measured by fNIRS with their recent temporal history were included in the feature space for further classification. The SVM was used as a classification scheme. The intra-subject classification accuracy was around 83.44% with the RBF kernel and 81.14% with the linear kernel, while the inter-subject classification accuracy was 87.5%. The results indicated a great potential of fNIRS to become a new technology for online deception detection.

Acknowledgement

This research was supported by the World Class University program funded by the Ministry of Education, Science and Technology through the National Research Foundation of Korea (grant no R31-20004).

Appendix. Questions used in the experimental protocol

'Watch' questions.

(1) Did you take the watch from the drawer?
(2) Is the watch in your envelope?
(3) Did you take the watch?
(4) Did you steal the watch?
(5) Was the watch stolen?
(6) Did you hide the watch?
(7) Do you know who took the watch?
(8) Is the watch with your possessions?
(9) Did you take a watch that is not yours?
(10) Is there a stolen watch in your envelope?
(11) Did you put the watch in your envelope?
(12) Did you hide the watch in your envelope?
(13) Did you remove a watch from the drawer?
(14) Did you steal a watch from the drawer?
(15) Did you place the watch in your envelope?
(16) Did you keep the watch in the drawer?
(17) Did you leave the watch in the drawer?
(18) Did the watch stay in the drawer?
(19) Was the watch moved from the drawer?
(20) Is the watch in the drawer?

'Ring' questions.

(1) Did you take the ring from the drawer?
(2) Is the ring in your envelope?
(3) Did you take the ring?
(4) Did you steal the ring?
(5) Was the ring stolen?
(6) Did you hide the ring?
(7) Is the ring with your possessions?
(8) Is there a stolen ring in your locker?
(9) Is there a stolen ring in your envelope?
(10) Did you take a ring that is not yours?
(11) Did you put the ring in your envelope?
(12) Did you hide the ring in your envelope?
(13) Did you remove a ring from the drawer?
(14) Did you steal a ring from the drawer?
(15) Did you place the ring in your envelope?
(16) Did you keep the ring in the drawer?
(17) Did you leave the ring in the drawer?
(18) Did the ring stay in the drawer?
(19) Was the ring moved from the drawer?
(20) Is the ring in the drawer?

References

Abdelnour A F and Huppert T 2009 Real-time imaging of human brain function by near-infrared spectroscopy using an adaptive general linear model *Neuroimage* **46** 133–43

Barbour R L, Graber H L, Pei Y L, Zhong S and Schmitz C H 2001 Optical tomographic imaging of dynamic features of dense-scattering media *J. Opt. Soc. Am.* A **18** 3018–36

Boas D A, Dale A M and Franceschini M A 2004 Diffuse optical imaging of brain activation: approaches to optimizing image sensitivity, resolution, and accuracy *Neuroimage* **23** S275–88

Brett A S, Phillips M and Beary J F 1986 Predictive power of the polygraph—can the lie-detector really detect liars *Lancet* **1** 544–7

Chang C C and Lin C J 2011 LIBSVM: a library for support vector machines *ACM Trans. Intell. Syst. Technol.* **2** 1–27

Coyle S M, Ward T E and Markham C M 2007 Brain–computer interface using a simplified functional near-infrared spectroscopy system *J. Neural Eng.* **4** 219–26

Cui X, Bray S and Reiss A L 2010 Speeded near infrared spectroscopy (NIRS) response detection *PLoS One* **5** 1–7

Elaad E 1997 Polygraph examiner awareness of crime-relevant information and the guilty knowledge test *Law Hum. Behav.* **21** 107–20

Elaad E and Benshakhar G 1991 Effects of mental countermeasures on psychophysiological detection in the guilty knowledge test *Int. J. Psychophysiol.* **11** 99–108

Elaad E and Benshakhar G 1997 Effects of item repetitions and variations on the efficiency of the guilty knowledge test *Psychophysiology* **34** 587–96
Farwell L A and Donchin E 1991 The truth will out—interrogative polygraphy (lie detection) with event-related brain potentials *Psychophysiology* **28** 531–47
Furedy J J and Benshakhar G 1991 The roles of deception, intention to deceive, and motivation to avoid detection in the psychophysiological detection of guilty knowledge *Psychophysiology* **28** 163–71
Ganis G, Kosslyn S M, Stose S, Thompson W L and Yurgelun-Todd D A 2003 Neural correlates of different types of deception: an fMRI investigation *Cerebral Cortex* **13** 830–6
Gratton G and Fabiani M 2001a The event-related optical signal: a new tool for studying brain function *Int. J. Psychophysiol.* **42** 109–21
Gratton G and Fabiani M 2001b Shedding light on brain function: the event-related optical signal *Trends Cogn. Sci.* **5** 357–63
Honts C R, Raskin D C and Kircher J C 1994 Mental and physical countermeasures reduce the accuracy of polygraph tests *J. Appl. Psychol.* **79** 252–9
Hu X S, Hong K S and Ge S S 2011 Recognition of stimulus-evoked neuronal optical response by identifying chaos levels of near-infrared spectroscopy time series *Neurosci. Lett.* **504** 115–20
Hu X S, Hong K S, Ge S S and Jeong M Y 2010 Kalman estimator- and general linear model-based on-line brain activation mapping by near-infrared spectroscopy *Biomed. Eng. Online* **9** 82
Huettel S A, Song A W and Mccarthy G 2008 *Functional Magnetic Resonance Imaging* (Sunderland, MA: Sinauer Associates)
Irani F, Platek S M, Bunce S, Ruocco A C and Chute D 2007 Functional near infrared spectroscopy (fNIRS): an emerging neuroimaging technology with important applications for the study of brain disorders *Clin. Neuropsychol.* **21** 9–37
Koizumi H, Yamamoto T, Maki A, Yamashita Y, Sato H, Kawaguchi H and Ichikawa N 2003 Optical topography: practical problems and new applications *Appl. Opt.* **42** 3054–62
Kozel F A, Johnson K A, Grenesko E L, Laken S J, Kose S, Lu X H, Pollina D, Ryan A and George M S 2009a Functional MRI detection of deception after committing a mock sabotage crime *J. Forensic Sci.* **54** 220–31
Kozel F A, Johnson K A, Laken S J, Grenesko E L, Smith J A, Walker J and George M S 2009b Can simultaneously acquired electrodermal activity improve accuracy of fMRI detection of deception *Soc. Neurosci.* **4** 510–7
Kozel F A, Johnson K A, Mu Q W, Grenesko E L, Laken S J and George M S 2004a Developing functional MRI detection of deception *Neuropsychopharmacology* **29** S84–5
Kozel F A, Johnson K A, Mu Q W, Grenesko E L, Laken S J and George M S 2005 Detecting deception using functional magnetic resonance imaging *Biol. Psychiatry* **58** 605–13
Kozel F A, Padgett T M and George M S 2004b A replication study of the neural correlates of deception *Behav. Neurosci.* **118** 852–6
Langleben D D, Loughead J W, Bilker W B, Ruparel K, Childress A R, Busch S I and Gur R C 2005 Telling truth from lie in individual subjects with fast event-related fMRI *Hum. Brain Mapp.* **26** 262–72
Langleben D D, Schroeder L, Maldjian J A, Gur R C, Mcdonald S, Ragland J D, O'brien C P and Childress A R 2002 Brain activity during simulated deception: an event-related functional magnetic resonance study *Neuroimage* **15** 727–32
Lee T M C, Liu H L, Tan L H, Chan C C H, Mahankali S, Feng C M, Hou J W, Fox P T and Gao J H 2002 Lie detection by functional magnetic resonance imaging *Hum. Brain Mapp.* **15** 157–64
Mohamed F B, Faro S H, Gordon N J, Platek S M, Ahmad H and Williams J M 2006 Brain mapping of deception and truth telling about an ecologically valid situation: functional MR imaging and polygraph investigation—initial experience *Radiology* **238** 679–88
Nunez J M, Casey B J, Egner T, Hare T and Hirsch J 2005 Intentional false responding shares neural substrates with response conflict and cognitive control *Neuroimage* **25** 267–77
Obrig H and Villringer A 2003 Beyond the visible—imaging the human brain with light *J. Cereb. Blood Flow Metab.* **23** 1–18
Perrey S 2008 Non-invasive NIR spectroscopy of human brain function during exercise *Methods* **45** 289–99
Phan K L, Magalhaes A, Ziemlewicz T J, Fitzgerald D A, Green C and Smith W 2005 Neural correlates of telling lies: a functional magnetic resonance imaging study at 4 tesla *Acad. Radiol.* **12** 164–72
Sitaram R, Caria A and Birbaumer N 2009 Hemodynamic brain–computer interfaces for communication and rehabilitation *Neural Netw.* **22** 1320–8
Sitaram R, Zhang H H, Guan C T, Thulasidas M, Hoshi Y, Ishikawa A, Shimizu K and Birbaumer N 2007 Temporal classification of multichannel near-infrared spectroscopy signals of motor imagery for developing a brain–computer interface *Neuroimage* **34** 1416–27
Spence S A, Farrow T F D, Herford A E, Wilkinson I D, Zheng Y and Woodruff P W R 2001 Behavioural and functional anatomical correlates of deception in humans *Neuroreport* **12** 2849–53
Spence S A, Hunter M D, Farrow T F D, Green R D, Leung D H, Hughes C J and Ganesan V 2004 A cognitive neurobiological account of deception: evidence from functional neuroimaging *Phil. Trans. R. Soc. Lond.* B **359** 1755–62
Tian F H, Sharma V, Kozel F A and Liu H L 2009 Functional near-infrared spectroscopy to investigate hemodynamic responses to deception in the prefrontal cortex *Brain Res.* **1303** 120–30
Toronov V Y, Zhang X and Webb A G 2007 A spatial and temporal comparison of hemodynamic signals measured using optical and functional magnetic resonance imaging during activation in the human primary visual cortex *Neuroimage* **34** 1136–48
Turnip A, Hong K S and Jeong M Y 2011 Real-time feature extraction of P300 component using adaptive nonlinear principal component analysis *Biomed. Eng. Online* **10** 83
Wolf M, Ferrari M and Quaresima V 2007 Progress of near-infrared spectroscopy and topography for brain and muscle clinical applications *J. Biomed. Opt.* **12** 062104